The pre-breakup stratigraphy and petroleum system of the Southern Jan Mayen Ridge revealed by seafloor sampling

Stéphane Polteau[1], Adriano Mazzini[2], Geir Hansen[3], Sverre Planke[1,2], Dougal A. Jerram[2,4,5], John Millett[1,6], Mansour M. Abdelmalak[1,2], Anett Blischke[7], Reidun Myklebust[8]

[1] Volcanic Basin Petroleum Research (VBPR), Oslo Science Park, 0349 Oslo, Norway.

[2] Centre for Earth Evolution and Dynamics (CEED), University of Oslo, 0315 Oslo, Norway.

[3] Applied Petroleum Technology AS, 0903 Oslo, Norway.

[4] DougalEARTH Ltd., Solihull B91 3NU, UK.

[5] Visiting research fellow, Earth, Environmental and Biological Sciences, Queensland University of Technology, Brisbane, QLD 4000, Australia.

[6] Department of Geology and Petroleum Geology, University of Aberdeen, AB24 3FX, UK.

[7] ISOR - Iceland Geosurvey, 108 Reykjavik, Iceland.

[8] TGS, Lensmannslia 4, 1386 Asker, Norway.

ABSTRACT

The Jan Mayen Microplate Complex (JMMC) in the NE Atlantic is interpreted to mostly consist of continental fragments with possible interstitial embryonic oceanic crust. A complex Cenozoic rifting history accompanied by extensive extrusive and intrusive volcanism have made the geological characterization of the JMMC challenging especially due to poor seismic imaging beneath the breakup basalt succession. The presence of continental crust in the JMMC is inferred by seismic and magnetic data, but ground truthing evidence have yet to be provided. Here, we present the results from a seafloor sampling campaign undertaken in 2011 on the Southern Jan Mayen Ridge complex. Seabed samples were recovered using a gravity corer and a dredge along 1000 m high escarpment with a 19° slope. Sampling locations were selected based on the interpretation of seismic profiles that suggest the presence of possible pre-breakup successions outcropping along this steep escarpment. Results include a sequence of samples with age diagnostic palynomorph assemblages ranging from Permian/Triassic

to Eocene, and including igneous samples related to the Early Eocene breakup volcanism. Importantly, samples were retrieved from hard substrate in an erosional gully lacking overburden sediments and have ages arranged in younging upward sequential order, supporting their in-situ position. The sampling results were integrated into a lithostratigraphic pseudo-well that can be used to constrain the evolution and breakup of the JMMC. Additionally, evidence for active migration of Jurassic sourced hydrocarbons comprise the first indication of a working hydrocarbon system, with important implications for the petroleum prospectivity of the Dreki area. Finally, these results confirm that the Southern Jan Mayen Ridge is indeed a sliver of continental crust.

Key words: *Jan Mayen Microplate Complex, seafloor sampling, NE Atlantic, Jurassic, petroleum system, sub-basalt, pre-breakup, breakup*

INTRODUCTION

Background and aims

Jan Mayen is an island in the NE Atlantic located between Iceland and Svalbard, and along with the surrounding ~550-km-long and 100-250 km-wide platform, is interpreted to mostly consist of continental fragments with possible interstitial embryonic oceanic crust (Auzende et al., 1980; Grønlie et al., 1979; Gudlaugsson et al., 1988; Myhre et al., 1984; Nunns, 1982; Skogseid and Eldholm, 1988; Torsvik et al., 2015). This enigmatic province is currently referred as the Jan Mayen Microplate Complex (JMMC; Gernigon et al., 2015; Schiffer et al., in press). Seismic mapping of the JMMC suggests the possibility of significant stratigraphy and basement structures beneath breakup-related volcanic rocks. The oldest penetrated sediments in DSDP (Deep Sea Drilling Program) Hole 349 from leg 38 on the Jan Mayen Ridge were post-breakup Middle Eocene (**Figure 1**; Talwani et al., 1976). The other direct indications for the presence of pre-breakup succession on the JMMC come from seafloor sampling conducted in 2010 and 2012 by the National Energy Authority of Iceland (NEA) and Norwegian Petroleum Directorate (NPD) in which an ROV (remotely operated underwater vehicle) collected late Permian-early Triassic to Oligocene-Miocene samples (Sandstå et al., 2012). However,

the presence of the pre-breakup successions is still debated because the Permian-Triassic samples were collected in the scree at the base of the escarpment, suggesting that these samples may not represent the in situ local geology of the ridge.

Without any borehole intersecting the sub-basalt stratigraphy on the JMMC, many questions remain as to the nature and age of the pre-Eocene stratigraphy, and in particular, whether the pre-breakup succession contains a working hydrocarbon system (Vis, 2017). In this contribution, we present the results from a seafloor sampling campaign (JMRS11, Jan Mayen Ridge Sampling 2011) along seismic line JM-17-85 (**Figure 1D**) where a 1 km high escarpment dipping by 19° offered the unique opportunity to recover pre-breakup in situ sub-cropping sediments and breakup related volcanic rocks using a gravity corer and dredge. The recovered material was mostly from truncated sequences outcropping at the seafloor for stratigraphy studies, and sampling concentrated below the basalt reflection to target pre-breakup strata (see **Figure 1**). In addition clay samples were collected for hydrocarbon seep studies to test for the presence of a possible working hydrocarbon system in the survey area. The goals of this manuscript are to describe the pre-breakup stratigraphic succession outcropping in the survey area, and to characterize the petroleum system identified in the Southern Jan Mayen Ridge.

Geological settings

The JMMC is a structural entity encompassing a segmented ridge complex, basins and a through (see **Figure 1**; e.g. Blischke et al., 2017; Gaina et al., 2009; Peron-Pinvidic et al., 2012). The JMMC is surrounded by oceanic crust, and may also extend towards Iceland to the south (see **Figure 1**; Blischke et al., 2017; Foulger, 2006; Torsvik et al., 2015). The JMMC is bounded to the north by the Jan Mayen Fracture Zone (JMFC), to the southeast by the Ægir Ridge, and to the northwest by the Kolbeinsey Ridge (**Figure 1**).

The JMMC is interpreted to have been part of the Møre Basin (e.g. Theissen-Krah et al., 2017) probably as a continuation of the south Gjallar and Rån ridges (Gernigon et al., 2015) prior to breakup

between Norway and Greenland in the earliest Eocene (e.g. Gaina et al., 2009). Fragments of the JMMC fringed the East Greenland margin until 52 Ma (Early Eocene) when the Reykjanes Ridge propagated northwards and detached the earliest fragment of the southern part of the JMMC from East Greenland after 47 Ma (Larsen et al., 2013; Torsvik and Cocks, 2016). During the Eocene and Oligocene, the JMMC is thought to have drifted westwards with the Greenland plate relative to the Eurasian plate. The complete separation of the JMMC from East Greenland took place after final ridge relocation in the late Oligocene to early Miocene, with the abandonment of the Ægir Ridge and the onset of spreading along the Kolbeinsey Ridge (Blischke et al., 2017; Vogt et al., 1970).

Extensive volcanic activity associated with continental breakup and the North Atlantic Igneous Province (Saunders et al., 1997) blanketed much of the region with extrusive basalts during the Late Paleocene - Early Eocene, whilst extensive intrusive sill complexes are also known (Blischke et al., 2017). Poor imaging below the volcanic cover caused early interpretations of seismic stratigraphy on the Jan Mayen Ridge to be largely limited to post-breakup reflections (Åkermoen, 1989). However, it is now accepted that the Jan Mayen Ridge in the northern part of the JMMC is underlain by continental crust (Breivik et al., 2012; Gaina et al., 2009; Grønlie and Talwani, 1978; Gudlaugsson et al., 1988; Kuvaas and Kodaira, 1997; Mjelde et al., 2007; Myhre et al., 1984; Skogseid and Eldholm, 1987). Today, improved imaging in reprocessed seismic data combined with deep seismic profiles and gravity/magnetic anomaly interpretations across the JMMC have revealed a complex system of crustal blocks which record up to six main phases of Cenozoic tectonism linked to regional unconformities (Blischke et al., 2017; Gaina et al., 2009; Gernigon et al., 2015). These interpretations are also consistent with observations from the conjugate NE Greenland and mid-Norway margins where pre-breakup sediments are imaged beneath the breakup basalt sequence (e.g. on the Vøring Marginal High; Abdelmalak et al., 2015; Abdelmalak et al., 2016a; Abdelmalak et al., 2016b; Planke et al., 2017).

METHODS

Seafloor sampling of the JMMC was undertaken by VBPR and TGS during a cruise in September 2011. The 55 m long Sermilik II trawler was used for the operations, with the site located across a steep escarpment along the seismic line JM-17-85 (see **Figure 1** for location). The Southern Jan Mayen Ridge was sampled and the recovered material was analyzed using the methods described below.

Sampling equipment and sample handling

A gravity corer and a dredge were both deployed during the sampling operations, and both were built and designed by Prof. Yngve Kristoffersen at the University of Bergen. The gravity core has a lead weight of 800 kg attached to a 3 m long carbon steel core barrel (**Figure** 2A and 2B). A transparent liner was inserted into the core barrel, and secured in place using a core catcher and cutting shoe (bit). The gravity corer was dropped in free fall from 50 m above the seafloor to maximize penetration into the seabed (**Figure** 2C). The contents of the bit were routinely sieved through a 1 mm mesh for identification of rock fragments enclosed in soft sediments (**Figure** 2D). The dredge consisted of an 80x50x40 cm steel frame with a chain bag lined with nylon netting (**Figure** 2B). The dredge was dragged along two overlapping 1.5 km-long profiles and allowed the recovery of rock fragments that would otherwise not be picked up by gravity coring (**Figure** 2E).

The GPS system on the ship was a Trimble NavTrac system, with antennae for GPS mounted on the monkey island. Correction signals ensured that the GPS was differential with error in position below 10 m. The position was logged in the coordinate systems WGS84, UTM31 in 10 km intervals during transit, and in navipack files during sampling. The recorded position of the sampled sites corresponds to the position of the trawl block used for coring at the moment of impact, while the dredging start/end points correspond to positions of the same trawl block when the ships started/stopped to follow the dredge profile (**Tables 1 and 2**).

Biostratigraphy

Biostratigraphy studies included seven gravity core and 15 dredge samples for palynology (**Tables 1 and 2**). Gravity core samples were initially selected for palynology if the contents of the bit

consisted of a lithified lithology, and if the sieved contents of the bit were dominated by one lithology. Dredge rock fragments were selected for palynology studies when they belonged to a lithological group.

Palynomorphs were identified using an Olympus BH-2 microscope equipped with a conventional camera. The palynological analyses were quantitative, and where possible, based on a minimum of 200 pollen counts. A general description of the kerogen composition for each sample included thermal alteration values according to a modified Thermal Alteration Index (TAI). TAI values were based on assessments of resistant organic material in the samples including pollen/spores, dinoflagellate cysts, and other algae and kerogen particles.

Organic geochemistry

The Applied Petroleum Technology (APT) laboratory follows the standard procedures from NIGOGA (Norwegian Industry Guide to Organic Geochemical Analysis), which defines analytical procedures, notation, and reporting guidelines (Weiss et al., 2000).

Rock fragments - Source rock evaluation

The 22 sedimentary rock fragments analyzed for biostratigraphy were also selected for total organic carbon (TOC) content (wt%), Rock-Eval pyrolysis, and for vitrinite reflectance analyses at the APT lab. Rock-Eval analysis by pyrolysis using a Rock-Eval 6 instrument (Vinci Technologies) provided hydrocarbon (HC) source characteristics and maturity levels of kerogen in the samples (Lafarge et al., 1999). Hydrogen Index (HI, mg HC/g TOC), Oxygen Index (OI, mg CO2/g TOC) and Tmax (expressed in °C) were determined. Tmax is the temperature at maximum pyrolytic hydrocarbon generation. It varies as a function of the natural thermal maturity of the organic matter (Espitalié et al., 1986). The vitrinite reflectance measurements analyses were performed on kerogen concentrates prepared following the kerogen isolation procedures outlined in Weiss et al. (2000) using a Zeiss Universal MPM03 photometer microscope.

Can samples - Seep studies

Four can samples were initially analyzed for headspace gas, followed by gas chromatography on extracted organic matter (GC of EOM). The two samples 13GC and 15GC with gas chromatograms displaying a thermogenic signature were further analyzed by gas chromatography mass spectrometry (GC-MS) on saturated and aromatic hydrocarbons.

Headspace gas was measured using a flame ionization detector (FID) for hydrocarbons, and two thermal conductivity detectors (TCD) for CH_4, H_2, CO_2, N_2 and O_2/Ar. The GC of EOM was measured using a HP5890 II instrument, and the GC-MS with a Micromass ProSpec high-resolution instrument, both following standard temperature programs.

Petrography and igneous geochemistry

Hand samples were cleaned and cut for examination. A set of three polished thin sections of basaltic rocks were prepared at APT. The textures were described and mineral phases identified using a standard optical microscopes at the University of Oslo. Hand specimens were also examined in detail using a binocular microscope. Geochemical analyses of chosen samples were also undertaken to help classify the igneous section. Analyses were carried out using an ARL 8420+ dual goniometer wavelength dispersive XRF spectrometer at the X.R.F. laboratory at the Department of Earth Sciences, Open University, Milton Keynes, UK. In addition, rare earth elements were also measured by ICP-MS at Royal Holloway, University of London, UK.

RESULTS

Sampling

A total of 11.11 m of sediment cores was retrieved from the 15 sampling stations. The majority of the cores were shorter than 1 m, except at stations 01GC, 02GC, 06GC, 13GC and 15GC (**Table 1**). At station 10GC the barrel was found empty and the core bit was damaged, probably indicating impact with a large clast preventing penetration of the gravity corer into the sediments. In two other instances (03GC, and 05GC) the gravity corer was retrieved with empty liners. The typical penetration depths of the gravity corer into soft recent seafloor sediments and drift range from ca. 1.5 to 3 m.

Three sites (01GC, 02GC, and 13GC) had the sieved contents of the bit consisting of a few grains of igneous and metamorphic rock fragments. In contrast, sites 04GC, 06GC, 09GC, 11GC, 12GC, 14GC, and 15GC had core recovery characterized by an upper unit consisting of soft sediment, and a bottom unit comprising lithified to semi-lithified rock fragments displaying variable degrees of alteration. These altered fragments were characterized by the presence of sedimentary laminations and organic-rich layers with abundant mica crystals (except at stations 06GC, 12GC, and 15GC).

Two dredge profiles were completed along the escarpment (**Table 2**). Profile 07D targeted the lowermost part of the ridge, and profile 08D covered the lower and mid-upper part of the escarpment (see **Figure 1**). The uppermost part of the escarpment, probably covered by recent sediments, was deliberately avoided as the seismic profile did not show any clear reflector intersecting the escarpment. The two dredge profiles provided a wider range in lithologies across the escarpment when compared to the gravity cores. The material recovered in both dredges is comparable in terms of lithological types. Dredge 08D was recovered full, and provided a larger amount of samples than dredge 07D ($1/10^{th}$ full). The combined recovery from the two dredges can be summarized in the following lithological groups.

- Group 1 (07D and 08D: 40%): Altered light brown to yellowish and often laminated shaly, silty, and sandy subcrops. The large majority of these lithotypes had significant amounts of 1-2 mm long muscovite crystals in their matrix. This lithology was similar to that recovered from gravity core sites 04GC, 06GC, 11GC, and 14GC.
- Group 2 (07D: 35%, 08D: 10%): Siltstone, some poorly cemented, others more lithified.
- Group 3 (07D and 08D: 10%): Different types of sandstone commonly laminated and poorly cemented. Some of the sandstones have carbonate cement and are very porous, while the large majority are dominated by a clay rich matrix.
- Group 4 (07D: 3%, 08D: 10%): Breakup volcanic rocks. These include freshly broken subaerial basalt, altered basalt, brecciated volcaniclastic and dolerite lithologies.
- Group 5 (07D and 08D: 1%): Carbonates and flint samples.

- Group 6 (07D: 1%, 08D: 5%): Shale fragments ranging in color from black to greenish were collected. Most samples reveal the presence of organic rich lenses along laminations emphasized by mica crystals. Commonly a silty fraction is also present. The specimens from this group are more indurated than those observed in Group 1, likely due to thermal alteration.
- Group 7 (07D: 10%, 08D: 24%): Heterogeneous mixture of high-grade metamorphic and igneous rocks consisting of sub-rounded and coarse grained gneisses and granitoids with occasional glacial striations.

Biostratigraphy

From the 22 sediment samples selected for palynology studies, 15 of the samples were dated based on their fossil content and/or organic facies (**Tables 1 and 2, and Figure 3**). The remaining seven samples were barren, very poor, and/or contained organic materials without any preserved microfossils, and hence could not be dated.

The immature Middle Eocene sample (14GC-Bit) in the upper portion of the ridge yielded a sparse but well preserved marine/oceanic Middle Eocene palynomorph assemblage, with numerous *Wetzeliella articulata pentagona*, *Systematophora placacantha* and *Areosphaeridium michoudii* (Eldrett et al., 2004; Nøhr-Hansen, 2003). The age can further be refined to the Lutetian (lower middle Eocene at 46-47 Ma; **Figure 4)**. This sample also contained a reworked and mature (TAI 3-4) Albian to Barremian foraminifera assemblage.

The Late Paleocene samples collected by dredging are rich in mature organic matter. However, identified palynomorphs are generally in a poor state of preservation, but were derived from a relatively narrow time interval in the earliest late Paleocene (Selandian, c 59 Ma). *Isabelidinium viborgense* (**Figure 4)** is a key fossil that is a marker for the sandy Våle Fm. in the North Sea, and is also one of the marker fossils for the Egga Member of the Tang Fm., deposited in the western parts of the Mid-Norway area (Lyck and Stemmerik, 2000). The samples are also relatively rich in reworked Late Cretaceous marine and terrestrial palynomorphs similar to the Egga Member. The depositional

environment is inferred to be marine with reworking of older Cretaceous strata likely derived from exposed highs or faults.

In addition, samples with Cretaceous, Jurassic and Permian-Triassic intervals have been identified in cores collected below the breakup basalt succession (**Figures 3 and 4)**. The Cretaceous samples (Maastrichtian-Campanian, Albian-Abtian and Barremian-Hauterivian) contained abundant and well-preserved microfossils (Bjærke, 1980; Dypvik et al., 2002; Håkanson et al., 1981), both for palynology and micropaleontology, but also contain a rich assemblage of reworked Jurassic and older elements suggesting a coastal depositional environment (Engkilde and Surlyk, 2003). The Middle Jurassic samples contained a few well-preserved key fossils from the Aalenian-Toarcian (**Figure 4)**, but alternatively *Nannoceratopsis gracilis* might instead be interpreted as reworked into fossil-barren Early Cretaceous beds.

Finally, the two gravity core samples 11GC and 12GC from the base of the escarpment (**Figure 3**) are nearly identical with respect to organic content, with a high proportion of inertinitic particles, cuticles and common fresh/brackish water alga *Botryococcus* spp (**Figure 4**). *Botryococcus* spp is a long ranging fossil, from the Permian or older and up to present, therefore the samples could not be dated based on their fossil content. However, the general organic facies is comparable to that often seen at the transition from the Permian and into the Triassic, perhaps on the Permian side because of the lack of marine elements (Mørk et al., 1990).

Overall, the four dated gravity core samples (**Table** 1) were arranged in the correct stratigraphic order, with post-breakup ages from samples recovered above the breakup basalts, Cretaceous age below the basalts, and Permian-Triassic age at the base of the escarpment. The results from the gravity corer were used to constrain the position of the dredge samples within the profile, and thus allowed the construction of a pseudo-well (**Figure 3**).

Petrography and igneous geochemistry

The igneous rocks sampled during the survey provide insights into the volcanic/igneous section exposed along the Jan Mayen Ridge. The recovered rock types include vesicular basalt, volcaniclastic breccias, and dolerite fragments (see **Figure 5**). Some of these rock fragments are particularly fresh.

The vesicular basalt samples (e.g. **Figure 5A and B**) display varying degrees of alteration. The most altered specimens display vesicles invariably filled with secondary minerals (amygdales) that display alignment and stretching in some of the samples. Areas of micro-crystalline groundmass and larger crystals can be seen in the weathered/altered examples, but no quenched glass was identified. One remarkably fresh example, as studied in thin section, shows olivine and plagioclase crystals (up to 2 mm) in a fine grained matrix. The olivine and plagioclase crystals are found as both individual phenocrysts and glomerocryst aggregates.

The dolerite fragments (**Figure 5C**) are medium grained and rich in olivine. The texture observed in these olivine dolerite specimens is an interlocking crystal framework of olivine and plagioclase crystals between 0.5 and 1 mm in size, with minor amounts of opaque minerals (possibly magnetite). Miarolitic cavities were observed in the samples; this texture highlights some exsolution of gases and indicate a possible shallow level of emplacement.

Volcaniclastic breccias (**Figure 5D**) are characterized by their dominant reddish color, and by their mixture of coarse- and fine-grained crystalline clasts set in a mixed sand grade matrix. The angular clasts consist of coarse-grained plagioclase-rich lava and fine-grained basalt fragments. Quenched glassy material was not observed in the clast rims or matrix precluding any evidence for rapid quenching.

Geochemical analysis was undertaken on four basalt samples. Three of the four sample analyses gave loss on ignition (LOI) of < 0.7 wt.% and major element totals > 99 wt. %, whereas the fourth sample (JMRS11-08D-Basalt), gave LOI of 3.8 wt.% due to alteration and the presence of interstitial hydrous minerals. Overall, we deem these to be acceptable values for weakly to moderately

altered basaltic rocks, however, we note the possibility that the more mobile elements may have been re-distributed in the most altered sample.

Geochemical analysis of the basaltic rocks shows a relatively high-magnesium content of ca. 7.43-11 wt.%, all plotting in the basalt field of the TAS classification (**Figure 5E**; Le Maitre, 1989). At least two suites of basalt, including a low TiO_2 (<1 wt.%) group and a high TiO_2 (<2 wt.%) group have been sampled. ICP-MS analyses for one sample in each of these groups reveals separate REE signatures (normalized to primitive mantle after McDonough and Sun, 1995), with the low TiO_2 sample recording depleted LREE e.g. La/Sm^N of 0.58, MORB-like signatures, whilst the high TiO_2 sample has a LREE enriched signature of e.g. La/Sm_N 3.02 (**Figure 5F**). These high and low TiO_2 samples, along with their equivalent REE signatures are broadly similar to the pre- and syn-rift magmas, respectively, recorded from the Faroe Islands and East Greenland (Larsen et al., 1989; Millett et al., 2017). Due to the limited number of analyses, we refrain from attempting further comparisons in this study. However, it is an important observation that both large and small fraction melts have been sampled in the study area.

Organic geochemistry

Four canned sediment samples were subjected to headspace gas analysis. The compositional analysis of the headspace gas shows that all samples are virtually barren in hydrocarbons and the relative proportions of nitrogen (N_2), oxygen (O_2) and carbon dioxide (CO_2) suggest air contamination.

The four shallow core samples were solvent-extracted. The yields were very low in all these cores, between 40 and 80 mg EOM/kg of extracted sediment. The gas chromatograms (**Figure 6**) typically display hydrocarbon distributions consistent with major contributions of bitumen from immature recent organic matter (ROM) in the C_{27}-C_{33} range. In addition to the overall ROM signature, samples 13GC and 15GC have chromatograms displaying a smooth *n*-alkanes distribution on top of a small hump of unresolved complex mixture (UCM) in the nC_{18} to nC_{26} range (30 and 50 min retention time). This combination of a UCM hump with a thermogenic envelope above suggest that traces of biodegraded thermogenic hydrocarbons are present in the sediment samples.

299 The distribution of *n*-alkanes can help differentiating between ROM and petrogenic
300 (thermogenic) migrated hydrocarbons. An odd or even C-number preference is invariably an indication
301 of immaturity, whereas a smooth *n*-alkane distribution with a carbon preference index (CPI) value close
302 to unity is characteristic of petrogenic hydrocarbons. Odd C-number *n*-alkane distributions (CPI >>1)
303 are caused by decarboxylation in oxic environments, and even C-numbered *n*-alkanes (CPI<<1) by
304 reduction (via alcohols) in anoxic settings. Samples 13GC and 15GC have the lowest CPI values, while
305 samples 01GC and 02GC CPI values are higher (**Table 3**).

306 The thermogenic signal identified in the gas chromatograms of samples 13GC and 15GC could
307 represent a) the contribution of ice-transported mature and immature organic matter, b) the mature
308 organic matter from the sub-cropping shales, or c) migrated thermogenic hydrocarbons. If the
309 thermogenic signal was from ice-transported organic matter, all four chromatograms should have
310 displayed the similar gas chromatogram patterns. Instead, the patterns are different depending on the
311 sample location, thus supporting a local origin for the thermogenic signal. The possibility that the
312 thermogenic signal is related to sub-cropping strata can be rules out since the TOC and Rock-Eval
313 results indicate that all of the outcropping rock fragments have a very poor source rock potential
314 (**Tables 1** and **2**). Therefore the slightly increased UCMs, thermogenic envelopes and low CPIs values
315 in samples 13GC and 15GC are evidences tentatively consistent with a minor petrogenic contribution
316 in sediments that are otherwise dominated by algal and higher plant sources. The other samples 01GC
317 and 02GC have their geochemical signatures characteristic of ROM source of indigenous bitumen with
318 very small UCM, no thermogenic envelopes, and relatively high CPI values.

319 The two samples 13GC and 15GC were selected for further analysis by GC-MS for both
320 saturated biomarkers and aromatic hydrocarbon distributions. The visual inspection of the mass
321 chromatograms (**Figure 7**) indicates that the samples contain only low yields of biomarkers and
322 aromatic hydrocarbons. Chromatograms of the triterpanes, however, show that the tricyclic terpanes
323 (cheilanthanes) occur relatively prominently compared to the pentacyclic terpanes (**Figure 7a**).

Summary and appraisal of results

High-resolution bathymetry maps of the Jan Mayen Ridge imaged clear erosive gullies distributed along the escarpment (**Figure 1**). These gullies suggest that erosional processes are active in the steep slopes where deposition of thick hemipelagic clays, capping subcropping strata, is effectively prevented. The presence of gullies further suggests that much of the dislodged material would be transported to the base of the escarpment. The short recoveries of the gravity cores consisted mainly of poorly lithified silty muscovite-rich shales interpreted as altered in situ strata. These altered rocks display well-preserved sedimentary structures and laminations that would not have formed in this present dynamic slope environment. These altered subcrop lithologies were also recovered in the dredge profiles, together with additional rock types including altered sediments, breakup related volcanic rocks, shales, siltstones, sandstones, carbonate rocks, and ice-rafted debris.

Critically, the rock fragments interpreted to be in situ are arranged in a sequential order, with the oldest sediments recovered at the base and the youngest at the top of the ridge. This normal age progression, hard nature of the substratum, and truncated seismic reflectors at the seabed collectively provide strong evidence supporting that the majority of the sampled rocks consist of in situ sedimentary strata outcropping at the seabed. The igneous units provide additional support for in situ sampling as many samples are extremely fresh, and have clearly not undergone significant weathering and transport.

We cannot entirely exclude that some of the gravity core samples have incorporated ice-rafted material. However, the lack of a random age distribution of samples along the profile does not support glacial transport from distant areas. In the Jan Mayen sub-marine slope system, ice rafted material along with locally mass wasted deposits will accumulate as wedges at the base of the slope on the basin floor. Therefore, the risk of sampling rocks that are not fully in-situ naturally increases towards the base of the slope. Finally, and of critical importance, the evidence supporting ongoing hydrocarbon

migration cannot be related to ice-rafted debris, and hence highlight that pre-breakup source rocks in the oil window are present in the JMMC.

DISCUSSION

Pre-breakup section

The presence of pre-breakup rocks on the JMMC is supported by the Cretaceous, Jurassic and Permian-Triassic biostratigraphic ages obtained from the gravity corer and dredge samples (**Figure 3**). Therefore the sampling reveals a highly condensed pre-breakup Mesozoic sequence (**Figure 3**), unless the lowermost Permian-Triassic samples were instead transported by local and/or ice-rafted debris and deposited at the base of the escarpment. Although drilling would be the ultimate test to confirm the presence and nature of the Mesozoic sequence, hydrocarbon migration and stratigraphic studies support the presence of pre-breakup strata along the sampling profile below the top basalt reflection (red line in **Figure 3**).

The study of the geochemical parameters and biomarkers from the samples 13GC and 15GC with a thermogenic signature can further characterize the depositional environment, maturity, and age of the source for the migrated hydrocarbons. Despite the low biomarkers abundance and yield, their pattern support an anoxic depositional environment for the source (type II or II/III kerogen). These conditions are interpreted from the Pr/Ph ratio, the Pr/nC$_{17}$ versus Ph/nC$_{18}$, CPI, and relative abundance of C$_{27}$, C$_{28}$ and C$_{29}$ steranes and of C$_{29}$, C$_{30}$ and C$_{31}$ hopanes (**Table 3**). The hopane and sterane maturity suggests that the hopane isomerization is near equilibrium, whereas sterane isomerization is incomplete, tentatively suggesting that the samples contain hydrocarbons from a source that have reached a vitrinite reflectance equivalence of about 0.6%. The maturity level is supported by observations from the aromatic hydrocarbon calculated from MPI1 values (after Radke and Welte, 1983; **Table 3**). This maturity level is also consistent with early maturity/onset of the oil window.

372 The age of the source can be determined by using the C_{28}/C_{29} sterane ratio and the extended
373 tricycle terpane (ETR) ratio. The Palaeozoic classification results from consideration of the C_{28}/C_{29}
374 sterane ratio (Grantham and Wakefield, 1988). The extended tricyclic terpane ratio (ETR; Holba et al.,
375 2001) is based on the abundance of C_{28} and C_{29} cheilanthanes relative to 27Ts:

376 ETR = (28/3R + 28/3S + 29/3R + 29/3S) / (28/3R + 28/3S + 29/3R + 29/3S + 27Ts)

377 The ETR ratio is based on m/z 191 responses and is most useful for distinguishing Triassic from
378 Jurassic marine-sourced oils. In general, Triassic sourced oils have ETR ≥0.67 and Early Jurassic oils have
379 ETR ≤0.67. Middle to Late Jurassic oils exhibit ETR values ≤0.67 and mostly <0.55.

380 The sharp drop in the ETR at the end of the Triassic corresponds to a major mass extinction
381 that may have had an impact on the principal biological sources of cheilanthanes and possibly
382 Tasmanites. A subsequent lesser extinction in the Toarcian may have further adversely impacted upon
383 these source organisms, resulting in low ETR for oils generated from Middle-Upper Jurassic source
384 rocks. Abrupt positive excursions in ETR values over geological time occurred in the Precambrian,
385 Silurian, Devonian, Permian-Triassic, Late Cretaceous and Miocene. However, high ETR values can also
386 be the result of marine upwellings (especially the Permian and younger episodes) rather than being
387 specific to the Triassic (Holba et al., 2003).

388 The cross plot of [28ββ/ (28ββ+29ββ)] vs. ETR (Holba et al., 2001) shows that both 13GC and
389 15GC fall within the "maximum Jurassic range" zone of the plot (**Figure 8**). Although the shallow core
390 extracts are slightly skewed towards post Jurassic values of the sterane parameter, the apparently
391 significant humic contribution in these samples is expected to lower the 28ββ/(28ββ+29ββ) ratio.
392 Therefore, the most likely age of the hydrocarbon source is Jurassic. In addition, the presence of
393 17α(H)-28,30-dinorhopane (although in low yields) in samples 13GC and 15GC further support an
394 anoxic source equivalent to the Upper Jurassic in the Barents and Norwegian Sea (Draupne and
395 Hekkingen formations). The anoxic Triassic Kobbe/Steinkobbe source rock is considered unlikely here

as, if present in the Southern Jan Mayen Ridge, it may be too deeply buried to generate hydrocarbons at a vitrinite reflectance equivalence of 0.6 %.

Breakup section

The age of the breakup volcanic section is constrained by the enclosing formations that were sampled and dated, with the thermally mature Late Paleocene samples (Selandian at 59.2 Ma; time scale from Gradstein et al., 1994) at the base and the immature Middle Eocene samples (Lutetian at 47 Ma) above (**Figure 3**). The position of the breakup-related volcanic samples within the profile is interpreted from the seismic data as a characteristic high amplitude reflection (red line in **Figure 3**) representing the extension of the SDRs towards the escarpment.

The vesicles observed in the basalt samples indicate active magma degassing due to pressure release near the surface. The alignment and stretching of vesicles are similar to those typically found in modern pāhoehoe lava crusts. Furthermore, the absence of any quenched glass is also consistent with the sub-aerial emplacement of lava flows without any interaction with water. The occurrence of glomerocrysts indicates that the lava flows were sourced from shallow magma chambers where olivine and plagioclase crystals were incorporated into cumulate aggregates (e.g. Jerram et al., 2003).

The presence of volcaniclastic rocks can have significant implications if they are the result of direct fragmentation of juvenile magma such as hyaloclastites or ignimbrites, or the result of reworked fragments of volcanically derived material (e.g. Millett et al., 2015; Watton et al., 2013). The lack of glassy material and the mixed nature of the clasts suggest that the volcaniclastic breccias are likely the reworked product of nearby exposed volcanic edifices and not primary fragmentation.

The relatively fine-grained nature of the olivine dolerite specimens supports the notion that it is likely to be a small volume intrusion. The presence of miarolitic cavities, which form due to exsolution of a fluid phase under low confining pressure, provides further evidence of crystallization occurring at a shallow depth possibly in the region of < 1-2 km.

In summary, the breakup volcanic section is interpreted to be approximately 100 m thick, and consists of stacked lava flows with hiatuses in volcanic activity marked by the deposition of volcaniclastic breccia units (**Figure 9**). Depending on the nature of the lava facies e.g. compound braided or simple tabular, it may be inferred that somewhere in the region of five to a few 10's of lava flows make up the sampled volcanic sequence based on observations from similar plateau sequences (e.g. Jerram, 2002). Olivine dolerite samples likely represent the sub-volcanic portion of the flows and may have acted as feeder dykes and/or sills.

Regional implications

The results of this study provide important new insights into the complex breakup history of the NE Atlantic (Blischke et al., 2017; Gaina et al., 2009; Gernigon et al., 2015). This contribution is also highly relevant for evaluating the hydrocarbon prospectivity of the JMMC but also of the conjugate outer Mid-Norwegian Margin (e.g. outer Møre Basin; Nirrengarten et al., 2014; Theissen-Krah et al., 2017). Furthermore, the sampled stratigraphic information provides a valuable calibration for mapping and interpreting seismic data within this area.

The igneous samples we retrieved can also be used to interpret and map more confidently the different volcanic facies imaged in the seismic data along the JMMC. In addition, these results can help constrain the volume, style and distribution of magmatism during continental breakup within this relatively under-investigated region of the North Atlantic Igneous Province (e.g. Abdelmalak et al., 2016a; Håkanson et al., 1981; Jerram et al., 2009; Planke et al., 2017). Furthermore, these magmatic processes and deposits have a direct influence on the petroleum system in the JMMC area (e.g. Reynolds et al., 2017; Senger et al., 2017).

CONCLUSIONS

This contribution presents new data from seafloor samples collected with a gravity corer and a dredge along a steep escarpment on the Southern Jan Mayen Ridge. The results document breakup and pre-breakup successions and a working Jurassic petroleum system.

In detail, the breakup volcanic succession consists of alternating layers of volcaniclastic breccia and olivine basalt flows. This extrusive package was fed by shallow level intrusions of olivine dolerite. These shallow intrusions increased the thermal maturity of recovered late Paleocene sediments in their contact metamorphic aureoles. The 59-47 Ma age range of the volcanic is constrained by the biostratigraphic age of the enclosing Selandian and Lutetian strata. The sub-basalt pre-breakup succession consists of Mesozoic and possibly Paleozoic strata. Cretaceous and Jurassic sediments were identified in the stratigraphic samples based on their palynomorph assemblages, and Permian-Triassic samples on their organic facies. This Mesozoic succession may be condensed if the Permian-Triassic sediments sampled at the base of the escarpment are in situ. Active migration of thermogenic hydrocarbon was identified in seabed sediments using organic geochemistry. Geochemical parameters and biomarkers extracted from the migrated hydrocarbons indicate a source rock equivalent in terms of age and anoxic depositional environment to the upper Jurassic Draupne Fm. in the Northern North Sea-Norwegian Sea, and Hekkingen Fm. in the Barents Sea.

The recovered pre-breakup successions and identified working Jurassic petroleum system in the central part of the JMMC confirm that a sliver of continental crust is present in the Southern Jan Mayen Ridge. Furthermore, these results have implications in terms of paleogeography and petroleum systems for the conjugate Møre Marginal Plateau and Rån Ridge in the outer Møre and Vøring basins, respectively. Finally, this study shows that seafloor sampling is a robust and simple method well adapted for frontier basins where geological data are scarce and greatly needed.

ACKNOWLEDGMENTS

The authors would like to acknowledge the contribution from the vessel's crew (captain I. Rasmussen) and operator (Thor Ltd), the two surveyors (K. Høysæth and H.B. Bortne), and two sampling assistants (F. Gausepohl and A.-M. Voelsch). Sverre Planke and Dougal Jerram are partly funded through a Norwegian Research Council Centers of Excellence project (project number 223272, CEED). Adriano Mazzini is funded by the European Research Council under the European Union's

Seventh Framework Programme Grant agreement n° 308126 (LUSI LAB project, PI A. Mazzini). TGS and VBPR funded the cruise and allowed the publication of the data and interpretation. Steve Killops from APT refined our interpretation of the biomarker data. The reviewers and the editor are also thanked for their constructive comments. Finally, this article is dedicated to the biostratigrapher Haavard Selnes who sadly passed away in 2015.

REFERENCES

Abdelmalak , M.M., Andersen, T.B., Planke, S., Faleide, J.I., Corfu, F., Tegner, C., Shephard, G.E., Zastrozhnov, D., Myklebust, R., 2015. The ocean-continent transition in the mid-Norwegian margin: insight from seismic data and an onshore Caledonian field analogue. Geology 43, 1011-1014.

Abdelmalak, M.M., Meyer, R., Planke, S., Faleide, J.I., Gernigon, L., Frieling, J., Sluijs, A., Reichart, G.J., Zastrozhnov, D., Theissen-Krah, S., Said, A., Myklebust, R., 2016a. Pre-breakup magmatism on the Vøring Margin: Insight from new sub-basalt imaging and results from Ocean Drilling Program Hole 642E. Tectonophysics 675, 258-274.

Abdelmalak, M.M., Planke, S., Faleide, J.I., Jerram, D.A., Zastrozhnov, D., Eide, S., Myklebust, R., 2016b. The development of volcanic sequences at rifted margins: New insights from the structure and morphology of the Vøring Escarpment, mid-Norwegian Margin. Journal of Geophysical Resarch Solid Earth 121.

Auzende, J.M., Beuzart, P., Bonnin, J., Olivet, J.L., Sischler, B., Unternehr, P., 1980. Mode de dislocation des continents lors des stades initiaux d´ouverture. 8eme Réunion des Sciences de la Terre de la Société Géologique de France, 18 pp.

Bjærke, T., 1980. Mesozoic Palynology of Svalbard V. – Dinoflagellates from the Agardhfjellet Member (Middle and Upper Jurassic) in Spitsbergen. Norsk Polarinstitutt Skrifter 172, 145-167.

Blischke, A., Gaina, C., Hopper, J.R., Péron-Pinvidic, G., Brandsdóttir, B., Guarnieri, P., Erlendsson, Ö., Gunnarsson, K., 2017. The Jan Mayen microcontinent: an update of its architecture, structural development and role during the transition from the Ægir Ridge to the mid-oceanic Kolbeinsey Ridge. Geological Society, London, Special Publications 447, 299-337.

Breivik, A.J., Mjelde, R., Faleide, J.I., Murai, Y., 2012. The eastern JanMayen microcontinent volcanic margin. Geophysical Journal International 188, 798-818.

Dypvik, H., Håkansson, E., Heinberg, C., 2002. Jurassic and Cretaceous palaeogeography and stratigraphic comparisons in the North Greenland-Svalbard region. Polar Research 21, 91-108.

Eldrett, J.S., Harding, I.C., Firth, J.V., Roberts, A.P., 2004. Magnetostratigraphic calibration of Eocene-Oligocene dinoflagellate cyst biostratigraphy from the Norwegian-Greenland Sea. Marine Geology 204, 91-127.

Engkilde, M., Surlyk, F., 2003. Shallow marine syn-rift sedimentation: Middle Jurassic Pelion Formation, Jameson Land, East Greenland. Geological Survey of Denmark and Greenland Bulletin 1, 813-863.

Espitalié, J., Deroo, G., Marquis, F., 1986. La pyrolyse Rock-Eval et ses applications. Part III. Revue Institut Français de Pétrole 41, 467-481.

Foulger, G.R., 2006. Older crust underlies Iceland. Geophysical Journal International 165, 672-676.

Gaina, C., Gernigon, L., Ball, P., 2009. Palaeocene-Recent plate boundaries in the NE Atlantic and the formation of the Jan Mayen microcontinent. Journal of the Geological Society 166, 601-616.

Gernigon, L., Blischke, A., Nasuti, A., Sand, M., 2015. Conjugate volcanic rifted margins, seafloor spreading, and microcontinent: Insights from new high-resolution aeromagnetic surveys in the Norway Basin. Tectonics 34, 907-933.

Gradstein, F.M., Agterberg, F.P., Ogg, J.G., Hardenbol, J., Van Veen, P., Thierry, J., Huang, Z., 1994. A Mesozoic time scale. journal of geophysical research 99, 24051-24074.

Grantham, P.J., Wakefield, L.L., 1988. Variations in the sterane carbon number distributions of marine source rock derived crude oils through geological time. Organic Geochemistry 12, 61-73.
Grønlie, G., Chapman, M., Talwani, M., 1979. Jan Mayen Ridge and Iceland Plateau: Origin and evolution. Norsk Polarinst Skrifter 170, 25-47.
Grønlie, G., Talwani, M., 1978. Geophysical Atlas of the Norwegian-Greenland Sea. Lamont-Doherty Geological Observatory, Palisades, N.Y.
Gudlaugsson, S.T., Gunnarsson, K., Sand, M., Skogseid, J., 1988. Tectonic and volcanic events at the Jan Mayen Ridge microcontinent., in: Morton, A., Parson, L. (Eds.), Early Tertiary Volcanism and the Opening of the NE Atlantic. Geological Society Special Publication, pp. 85-93.
Holba, A.G., Ellis, L., Dzou, L.I.P., Hallam, A., Masterson, W.D., Francu, J., Fincannon, A.L., 2001. Extended tricyclic terpanes as age discriminators between Triassic, Early Jurassic, and Middle–Late Jurassic oils. , 20th International Meeting on Organic Geochemistry, Nancy, France, pp. 10-14.
Holba, A.G., Zumberge, J., Huizinga, B.J., Rosenstein, H., Dzou, L.I.P., 2003. Extended tricyclic terpanes as indicators of marine upwelling. Abstract OXX., 21st International Meeting on Organic Geochemistry, Krakow, p. 131.
Håkanson, E., Birkelund, T., Piasecki, S., Zakharov, V., 1981. Jurassic – Cretaceous boundary strata of the extreme Arctic (Peary Land, North Greenland). Bull. Geol. Soc Denmark 30, 11-42.
Jerram, D.A., 2002. Volcanology and fades architecture of flood basalts. Volcanic Rifted Margins 362, 119.
Jerram, D.A., Cheadle, M.J., Philpotts, A.R., 2003. Quantifying the building blocks of igneous rocks: are clustered crystal frameworks the foundation? Journal of Petrology 44, 2033-2051.
Jerram, D.A., Single, R.T., Hobbs, R.W., Nelson, C.E., 2009. Understanding the offshore flood basalt sequence using onshore volcanic facies analogues: an example from the Faroe–Shetland basin. Geological Magazine 146, 353-367.
Kuvaas, B., Kodaira, S., 1997. The formation of the Jan Mayen microcontinent: the missing piece in teh continental puzzle between the Møre-Vøring basins and East Greenland. First Break July, 239-247.
Lafarge, E., Marquis, F., Poillot, D., 1999. Rock-Eval 6 application in hydrocarbon exploration, production, and soil contamination studies. Revue Institut Français de Pétrole 56, 421-437.
Larsen, L.M., Pedersen, A.K., Sørensen, E.V., Watt, W.S., Duncan, R.A., 2013. Stratigraphy and age of the Eocene Igtertivâ Formation basalts, alkaline pebbles and sediments of the Kap Dalton Group in the graben at Kap Dalton, East Greenland. Bulletin of the Geological Society of Greenland 61, 1-18.
Larsen, L.M., Watt, W.S., Watt, M., 1989. Geology and petrology of the Lower Tertiary plateau basalts of the Scoresby Sund region, East Greenland. Geology of Greenland Survey Bulletin 157, 1-164.
Le Maitre, R.W., 1989. A classification of igneous rocks and glossary of terms. recommendations of the International Union of Geological Sciences. Subcommission on the systematics of igneous rocks, 1st ed. Blackwell Scientific Publications, Oxford.
Lyck, J.M., Stemmerik, L., 2000. Palynology and depositional history of the Paleocene? Thyra Ø Formation, Wandel Sea Basin, eastern North Greenland. Geology of Greenland Survey Bulletin 187, 21-49.
McDonough, W.F., Sun, S.S., 1995. The composition of the Earth. Chemical Geology 120, 223-253.
Millett, J.M., Hole, M.J., Jolley, D.W., Passey, S.R., 2017. Geochemical stratigraphy and correlation within large igneous provinces: The final preserved stages of the Faroe Islands Basalt Group. Lithos 286, 1-15.
Millett, J.M., Hole, M.J., Jolley, D.W., Schofield, N., Campbell, E., 2015. Frontier exploration and the North Atlantic Igneous Province: new insights from a 2.6 km offshore volcanic sequence in the NE Faroe–Shetland Basin. Journal of the Geological Society 173, 320-336.
Mjelde, R., Eckhoff, I., Solbakken, S., Kodaira, S., Shimamura, H., Gunnarsson, K., Nakanishi, A., Shiobara, H., 2007. Gravity and S-wave modelling across the Jan Mayen Ridge, North Atlantic; implications for crustal lithology. Marine Geophysical Researches 28, 27-41.
Myhre, A.M., Eldholm, O., Sundvor, E., 1984. The Jan Mayen Ridge: present status. Polar Research 2, 47-59.

566 Mørk, A., Os Vigran, J., Hochuli, P.A., 1990. Geology and palynology of the Triassic succession of
567 Bjørnøya. Polar Research 8.
568 Nirrengarten, M., Gernigon, L., Manatschal, G., 2014. Lower crustal bodies in the Møre volcanic rifted
569 margin: Geophysical determination and geological implications. Tectonophysics 636, 143-157.
570 Nunns, A., 1982. The structure and evolution of the Jan Mayen Ridge and surroundings regions., in:
571 Watkins, J.S., Drake, C.L. (Eds.), Studies in Continental Margin Geology. American Association of
572 Petroleum Geologists Memoirs, pp. 193-208.
573 Nøhr-Hansen, H., 2003. Dinoflagellate cyst stratigraphy of the 485 Palaeogene strata from the
574 Hellefisk-1, Ikermiut-1, Kangâmiut-1, Nukik-1, Nukik-2 and Qulleq-1 wells, offshore West Greenland.
575 Marine and Petroleum Geology 20, 987-1016.
576 Peron-Pinvidic, G., Gernigon, L., Gaina, C., Ball, P., 2012. Insights from the Jan Mayen system in the
577 Norwegian–Greenland Sea—II. Architecture of a microcontinent. Geophysical Journal International
578 191, 413-435.
579 Planke, S., Millett, J.M., Maharjan, D., Jerram, D.A., Abdelmalak, M.M., Groth, A., Hoffmann, J., Berdnt,
580 C., Myklebust, R., 2017. Igneous seismic geomorphology of buried lava fields and coastal escarpments
581 on the Vøring volcanic rifted margin. Interpretation 5, 1-42.
582 Radke, M., Welte, D.H., 1983. The methylphenanthrene index (MPI): a maturity parameter based on
583 aromatic hydrocarbons, in: Bjorøy, M.e.a. (Ed.), Advances in Organic Geochemistry 1981. John Wiley
584 and Sons, Chichester, pp. 504-512.
585 Reynolds, P., Planke, S., Millett, J.M., Jerram, D.A., Trulsvik, M., Schofield, N., Myklebust, R., 2017.
586 Hydrothermal vent complexes offshore Northeast Greenland: A potential role in driving the PETM.
587 Earth and Planetary Science Letters 467, 72-78.
588 Sandstå, N.R., Pedersen, R.B., Williams, R., Bering, D., Magnus, C., Sand, M., Brekke, H., 2012.
589 Submarine fieldwork on the Jan Mayen Ridge; integrated seismic and ROV-sampling., Nordic Winter
590 Meeting, Reykjavik, Iceland.
591 Saunders, A.D., Fitton, J.G., Kerr, A.C., Norry, M.J., Kent, R.W., 1997. The north Atlantic igneous
592 province, in: Mahoney, J.J., Coffin, M.F. (Eds.), Large Igneous Provinces: Continental, and Planetary
593 Flood Volcanism. American Geophysical Union, pp. 45-93.
594 Schiffer, C., Peace, A., Phethean, J., Gernigon, L., McCaffrey, K., Petersen, K.D., Foulger, G.R., in press.
595 The Jan Mayen Microplate Complex and the Wilson cycle. Geological Society London Special
596 Publications.
597 Senger, K., Millett, J., Planke, S., Ogata, K., Eide, C.H., Festøy, M., Galland, O., Jerram, D.A., 2017. Effects
598 of igneous intrusions on the petroleum system: a review. First Break 35, 47-56.
599 Skogseid, J., Eldholm, O., 1987. Early Cenozoic Crust at the Norwegian Continental Margin and the
600 Conjugate Jan Mayen Ridge. J. Geophys. Res. 92(B11), 11471-11491.
601 Skogseid, J., Eldholm, O., 1988. Early Cenozoic evolution of the Norwegian volcanic passive margin and
602 the formation of marginal highs., in: Morton, A.C., Parson, L.M. (Eds.), Early Tertiary volcanism and the
603 opening of the NE Atlantic. Geological Society Special Publication, pp. 49-56.
604 Talwani, M., Udintsev, G., White, S.M., 1976. Introduction and explanatory notes, Leg 38, Deep Sea
605 Drilling Project. , in: Talwani, M., Udintsev, G. (Eds.), Initial Reports of the Deep Sea Drilling Project.
606 U.S. Government Printing Office, Washington, pp. 3-19.
607 Theissen-Krah, S., Zastrozhnov, D., Abdelmalak, M.M., Schmid, D.W., Faleide, J.I., Gernigon, L., 2017.
608 Tectonic evolution and extension at the Møre Margin – Offshore mid-Norway. . Tectonophysics 721,
609 227-238.
610 Torsvik, T.H., Amundsen, H.E.F., Trønnes, R.G., Doubrovine, P.V., Gaina, C., Kusznir, N.J., Steinberger,
611 B., Corfu, F., Ashwal, L.D., Griffin, W.L., Werner, S.C., Jamtveit, B., 2015. Continental crust beneath
612 southeast Iceland. Proceedings of the National Academy of Sciences of the United States of America
613 112, E1818-E1827.
614 Torsvik, T.H., Cocks, L.R.M., 2016. Earth History and Palaeogeography. Cambridge University Press,
615 Cambridge.
616 Vis, G.-J., 2017. Geology and seepage in the NE Atlantic region. Geological Society, London, Special
617 Publications 447, 443-455.

618 Vogt, P.R., Ostenso, N.A., Johnson, G.L., 1970. Magnetic and bathymetry data bearing on seafloor
619 spreading north of Iceland. Journal of Geophysical Research 75, 903-920.
620 Watton, T.J., Jerram, D.A., Thordarson, T., Davies, R.J., 2013. Three-dimensional lithofacies variations
621 in hyaloclastite deposits. Journal of Volcanology and Geothermal Research 250, 19-33.
622 Weiss, H.M., Wilhelms, A., Mills, N., Scotchmer, J., Hall, P.B., Lind, K., Brekke, T., 2000. NIGOGA- The
623 Norwegian Industry Guide to organic Geochemical Analyses (online). Available from World Wide Web:
624 htttp://www.npd.no/engelsk/nigoga/default.htm. Norsk Hydro, Statoil, Geolab Nor, SINTEF Petroleum
625 Research and the Norwegian Petroleum Directorate, p. 102.
626 Åkermoen, T., 1989. Jan Mayen-ryggen: Et seismisk stratigrafisk og strukturelt studium. Univ. of Oslo,
627 Oslo, p. 174.

628

629

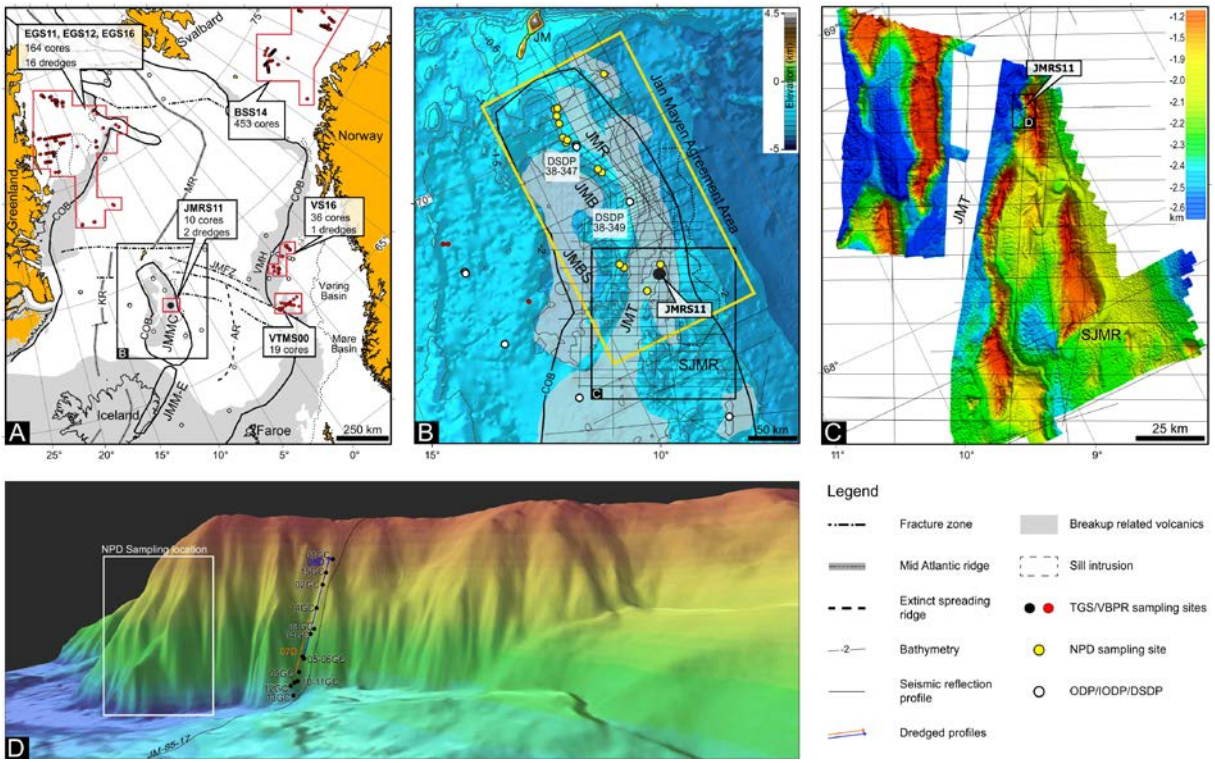

Figure 1. Regional setting and targeted area. **A**. Onshore and offshore distribution of the breakup related volcanics and sill intrusion in the North Atlantic Igneous Province (e.g., Abdelmalak et al., 2017). The map shows the location of the Jan Mayen Microplate Complex (JMMC) and additional VBPR/TGS sampling sites in the NE Atlantic (VTMS00, EGS11-12-16, BSS14, VS16), and scientific wells. **B**. Location of the JMRS11 and NPD (Norwegian Petroleum Directorate) seabed samples, scientific wells, and seismic data (GEBCO_2014 Grid bathymetry/topography http://www.gebco.net). The yellow box outlines the Jan Mayen Agreement Area. **C**. High-resolution bathymetry (A8-2008 multibeam dataset from http://www.landgrunnsvefsja.is/vefsja/icsp.html) of several segments forming the Southern Jan Mayen Ridge, with JM-85 surveys and location of the JMRS11 sites. **D**. 3D view of the JMRS11 sampling profile along seismic line JM-85-17 in erosive gully, and sampling area of NPD 2012 survey. AR: Aegir Ridge; COB: continent ocean boundary; JM: Jan Mayen Island; JMB: Jan Mayen Basin; JMBS: Jan Mayen Basin South; JMMC: Jan Mayen Microplate Complex; JMM-E: Jan Mayen Microplate Complex Extension; JMR: Jan Mayen Ridge; JMT: Jan Mayen Trough; KR: Kolbeinsey Ridge; MR: Mohn's Ridge; SJMR: Southern Jan Mayen Ridge; VMH: Vøring Marginal High.

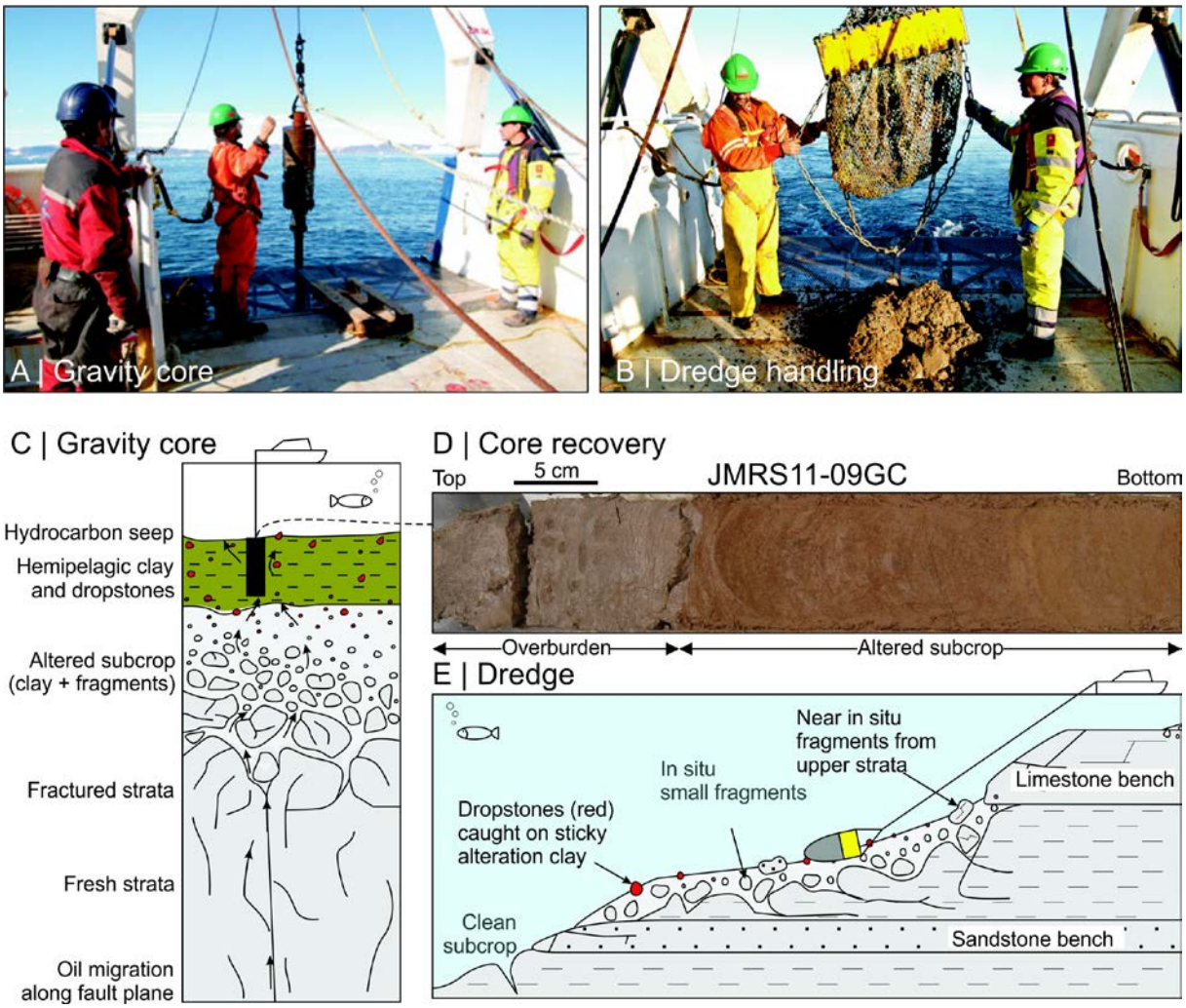

Fig. 2. Seabed sampling equipment used in this study. **A.** Handling of the gravity corer. **B.** Handling of the dredge on deck. **C.** Gravity coring is a point sampling method used for both stratigraphic and seep sampling. **D.** The semi-lithified sediments at the base of core recovery JMRS11-09GC were interpreted to represent altered subcropping strata and have a biostratigraphic, scale at the base is 5 cm interval. **E.** A dredge was used to sample rock fragments from outcropping strata along steep escarpments where the thickness of the overburden is limited.

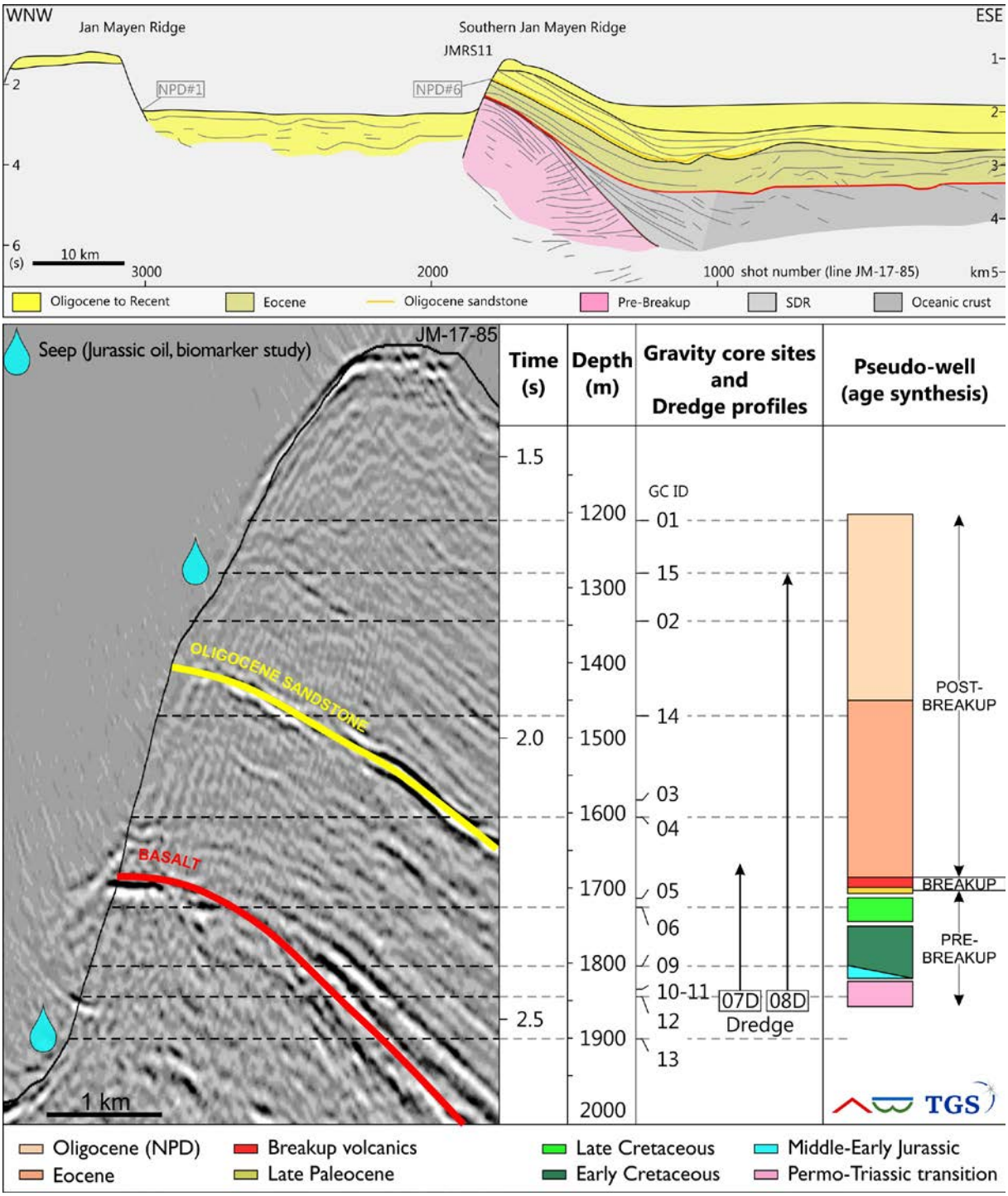

Figure 3. Interpretative geological cross-section along seismic line JM-85-17 (Åkermoen, 1989), and seismic section showing the location of the samples, biostratigraphic ages and results, and location of hydrocarbon seeps. NPD sites are shown, and include in situ Oligocene reservoir sandstone (NPD#6).

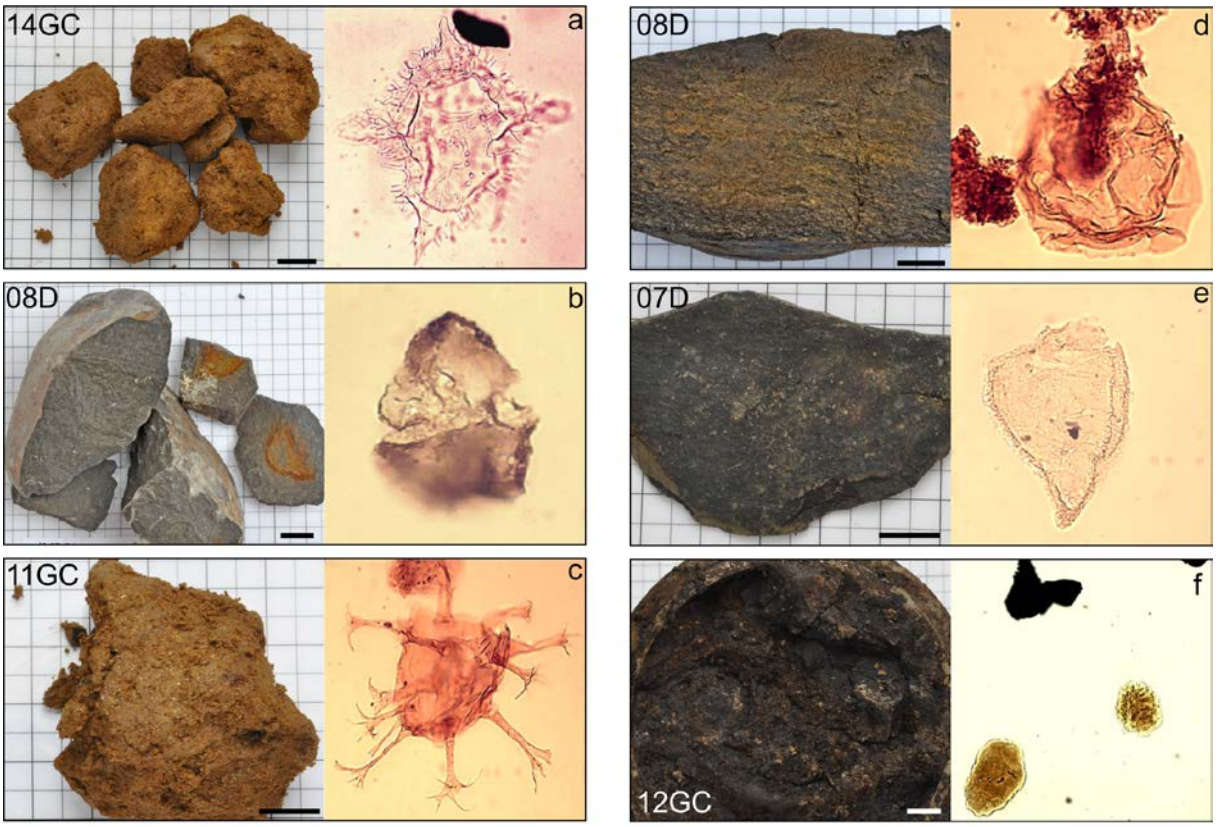

a. *Wetzeliella articulata pentagona* (Middle Eocene, Lutetian)
b. *Isabelidinium viborgense* (Late Paleocene, Selandian)
c. *Oligosphaeridium complex* (Albian-Aptian)
d. *Sirmiodinium grossii* (Barremian-Hauterivian)
e. *Nannoceratopsis gracilis* (Aalenian-Toarcian)
f. *Botryococcus* spp and inertinic facies (Permian-Triassic)

Figure 4. Microphotographs showing the key microfossils with their corresponding names and assigned biostratigraphic ages. Permian-Triassic ages were assigned based on the organic facies rather than age-diagnostic palynomorphs.

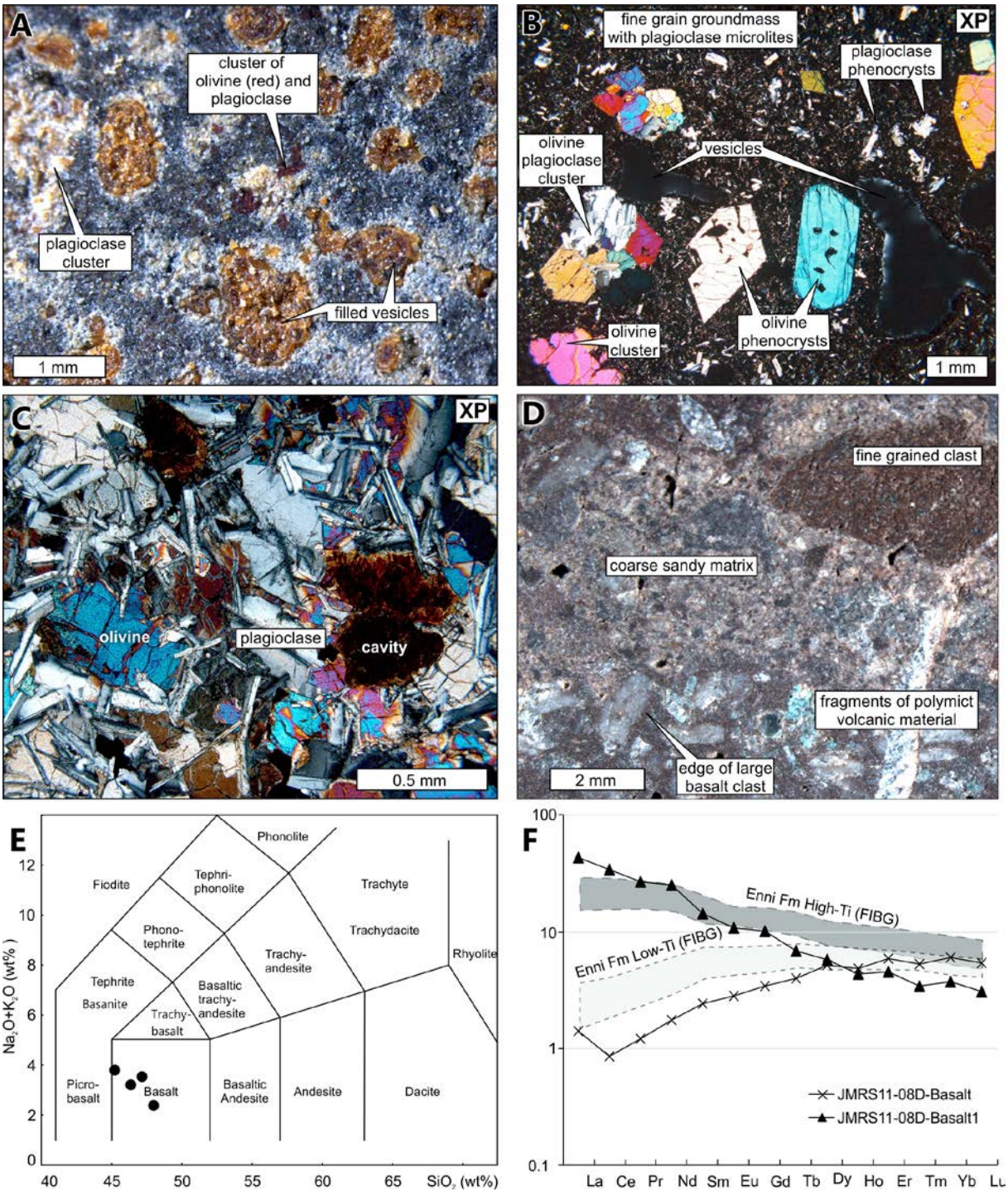

Figure 5. Petrology and classification of the igneous section. **A**. Binocular view of vesicular basalt. **B**. Thin section view in XP light of vesicular basalt sample. **C**. Detailed view in XP of dolerite. **D.** Example from the volcaniclastic sample. **E**. Total Alkali Silicate (TAS) classification showing the low alkali basalt composition of the analyzed samples. **F.** Rare Earth Element (REE) spider diagram normalized to primitive mantle (after McDonough and Sun, 1995) showing the Jan Mayen samples compared to data from the Enni Fm. of the Faroe Islands (Millets et al., 2017).

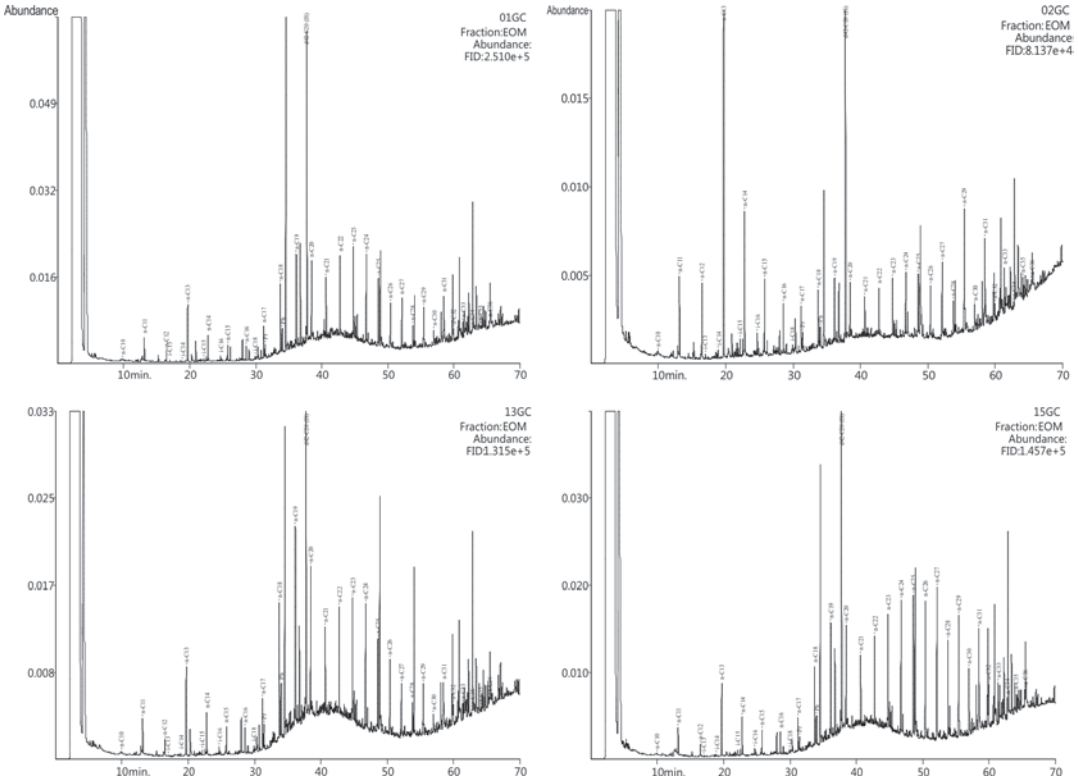

Figure 6. Gas chromatograms of the four analyzed samples. Samples 01GC and 02GC have a background signature while samples 13GC and 15GC display an apparent UCM and small thermogenic envelope. Peak identification follows NIGOGA procedures (Weiss et al., 2000).

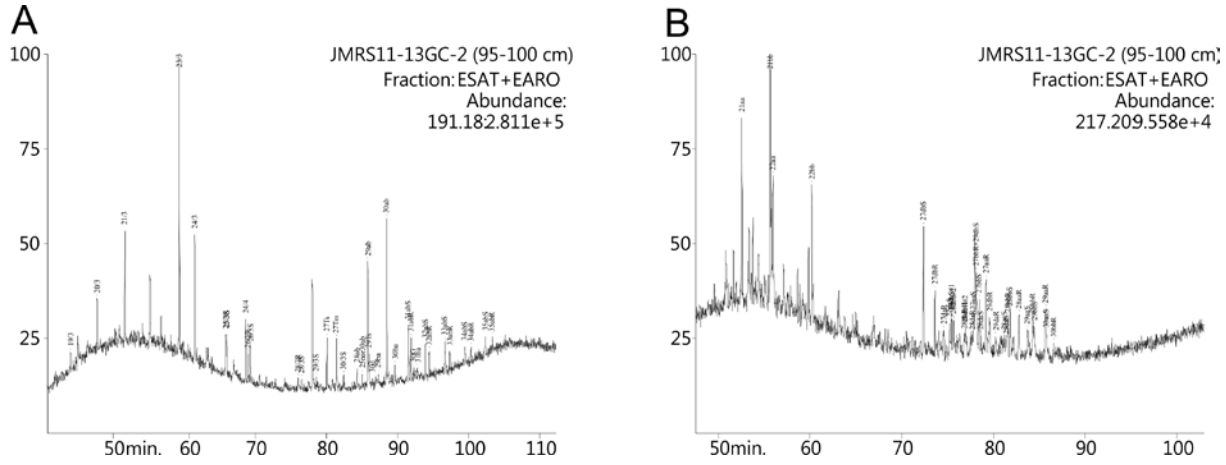

Figure 7. Examples of mass chromatograms (**A.** m/z191 and **B**. m/z 217) suggesting that the samples contain petrogenic hydrocarbons. Peak identification follows NIGOGA procedures (Weiss et al., 2000).

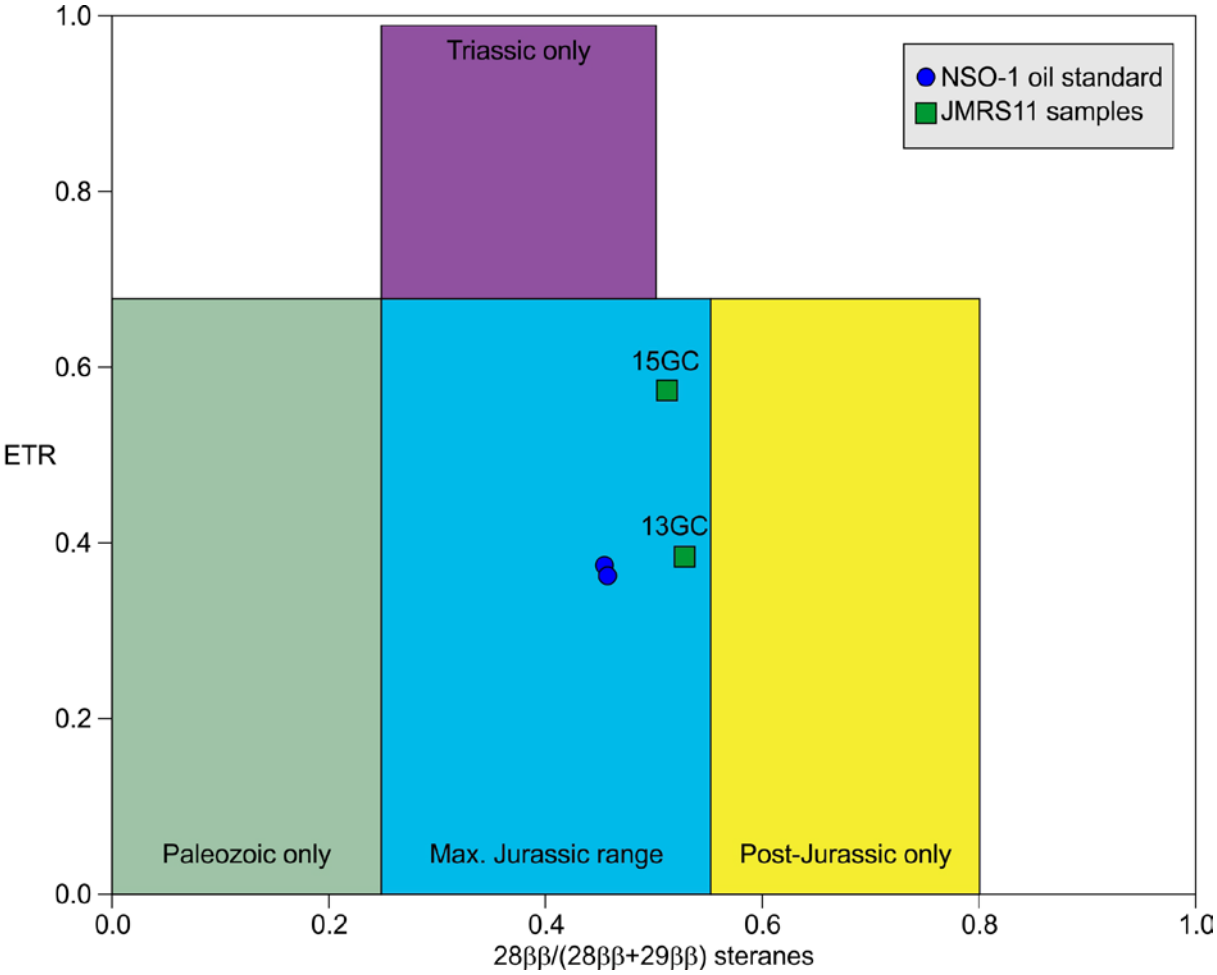

Figure 8. Cross plot of [28ββ/(28ββ+29ββ)] vs ETR as an age indication for sourcing of hydrocarbons. For the convenience of using a standard template, we use the x/(x+y) form of the ratio with values between 0 and 1 (although Holba et al. (2003) used x/y). The plot shows that the samples do not plot in the area that would be associated conclusively with a Paleozoic source, but within the range observed for the most common Jurassic sources.

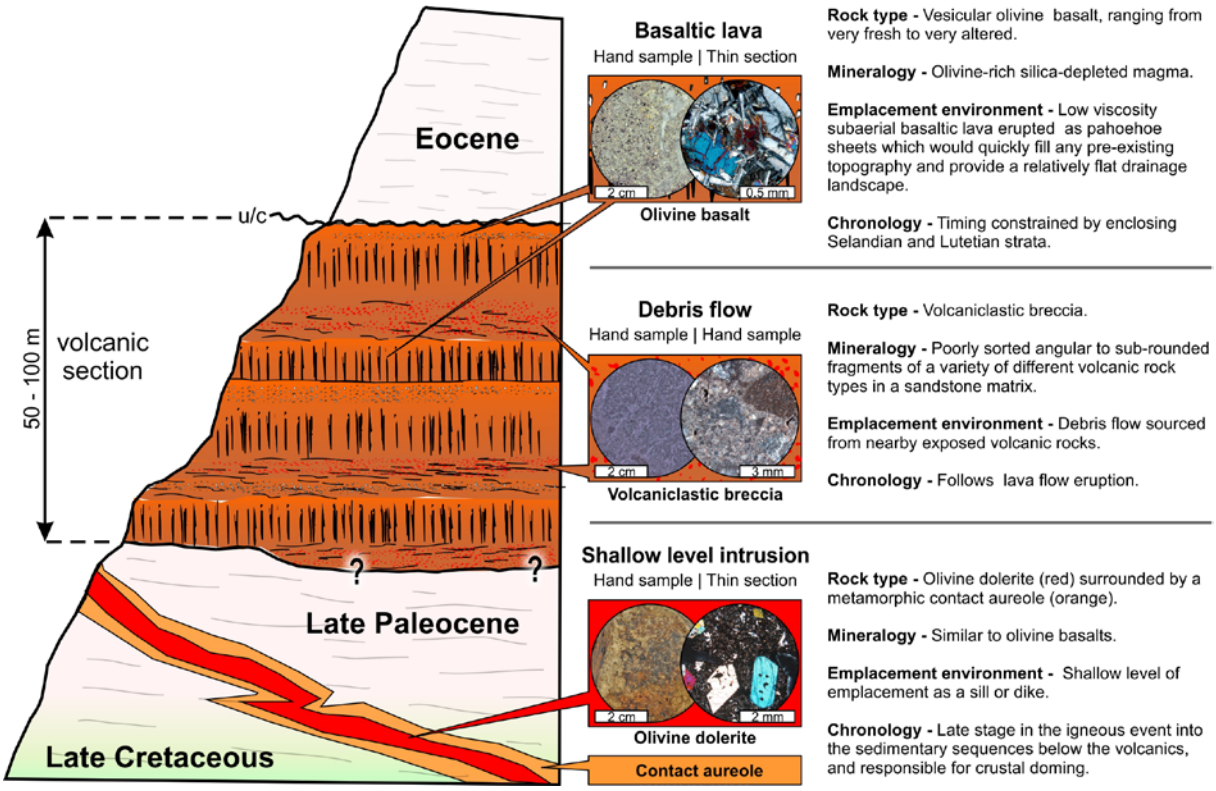

Figure 9. Schematic stratigraphic section interpreted from integrated sampling results.

Site	01GC	02GC	03GC	04GC	05GC	06GC	09GC	10GC	11GC	12GC	13GC	14GC	15GC
Latitude	68.494044	68.495690	68.497421	68.497910	68.498957	68.498953	68.500054	68.500571	68.500296	68.501364	68.500640	68.496937	68.495169
Longitude	8.234310	8.241399	8.253604	8.253758	8.259683	8.260343	8.266562	8.270674	8.269619	8.272428	8.275467	8.248262	8.237614
Water Depth (m)	1170	1300	1500	1500	1600	1550	1715	1691	1739	1737	1900	1370	1370
Recovery (cm)	190	156	0	39	0	105	46	0	48	63	215	45	208
Sieved Bit	-	-		brownish sandy clay with micas		yellowish clay/altered shale	brown shale with muscovite		yellowish brown shale with muscovite	black shale	-	brown shale with muscovite	black shale
TOC (wt%)	-	-		0.18		0.2	0.27		0.36	0.14	-	0.26	0.16
Tmax (°C)	-	-		611		604	467		472	609	-	498	611
HI (mg HC/g TOC)	-	-		494		1178	539		410	1846	-	584	1242
OI (mg CO/g TOC)	-	-		247		650	618		524	2266	-	748	1820
Vitrinite Reflectance (%)	-	-		Barren		0.53	Barren		0.39	Barren	-	1.47	Barren
Biostratigraphic Age	-	-		Pleistocene		Cretaceous	Jurassic		Permian/Triassic	Permian/Triassic	-	Eocene	Barren
TAI	-	-		0		3-(4)	3-2		2	2	-	1	-

Site	07D-1	07D-2	07D-3	07D-4	07D-6A	7D-11A	8D-1	08D-1A	08D-2	08D-2A	08D-4	08D-4A	08D-5	08D-8A	08D-9A
TOC (wt%)	1.02	2.14	0.15	0.22	0.65	0.47	0.47	0.75	0.15	0.27	0.87	0.13	0.38	0.68	0.26
Tmax (°C)	526	611	360	475	461	446	612	439	475	492	608	602	611	439	497
HI (mg HC/g TOC)	8	10	7	9	40	66	73	37	298	94	55	146	56	41	101
OI (mg CO/g TOC)	47	51	617	245	93	98	985	77	470	26	59	222	53	75	70
Vitrinite Reflectance (%)	4.41	1.02	Barren	Barren	0.63	0.61	Barren	0.62	0.55	Barren	4.93	0.65	Barren	Barren	0.96
Biostratigraphic Age	Jurassic	Cretaceous	Barren	Barren	Cretaceous	Cretaceous	Barren	Cretaceous	Barren	Barren	Jurassic	Barren	Jurassic	Cretaceous	Late Paleocene
TAI	3-2	4-5			4-5	4-5		3-(4)			3-2		3-2	3-(4)	4-5

Dredge 07D	Latitude:	SOL:68.500334	EOL:68.497467	Longitude:	SOL:8.267352	EOL:8.250918	Water Depth (m)	SOL:2550 EOL:1463	Recovery (cm)	1/10 of dredge
Dredge 08D	Latitude:	SOL:68.499291	EOL:68.494406	Longitude:	SOL:8.261019	EOL:8.232916	Water Depth (m)	SOL:2475 EOL:1188	Recovery (cm)	full dredge

Sample	CPI	Pr/nC_{17}	Ph/nC_{18}	(Pr/nC_{17})/(Ph/nC_{18}))	Pr/Ph	nC_{17}/(nC_{17}+nC_{27})	MPI1	%C27Iso	%C28Iso	%C29Iso	%C29Hops	%C30Hops	%C31Hops
01GC	1.67	0.63	0.59	1.07	0.51	0.35							
02GC	2.38	0.53	0.54	0.98	0.95	0.38							
13GC	1.36	0.69	0.6	1.14	0.45	0.46	0.50	45.63	27.38	26.98	0.48	0.75	0.33
15GC	1.37	0.61	0.56	1.09	0.52	0.18	0.42	42.92	27.09	29.99	0.50	0.63	0.39
NSO-1	1.02	0.59	0.46	1.29	1.51	0.78	0.60	34.11	30.24	35.66	0.24	0.95	0.47

MPI1 = 1.5(2MP + 3MP) / (P + 1MP + 9MP) P: Phenanthrene; MP: Methylphenanthrene

Steranes m/z 218: % C27Iso = 100*(27ββR+27ββS)/(27ββR+27ββS+28ββR+28ββS+29ββR+29ββS)

Steranes m/z 218: % C28Iso = 100*(28ββR+28ββS)/(27ββR+27ββS+28ββR+28ββS+29ββR+29ββS)

Steranes m/z 218: % C29Iso = 100*(29ββR+29ββS)/(27ββR+27ββS+28ββR+28ββS+29ββR+29ββS)

Hopanes 29Hops = C_{29} Hopane/ (C_{29} + C_{30} +C_{31} 22S and C_{31} 22R)Hopanes

Hopanes 30Hops = C_{30} Hopane/ (C_{29} + C_{30} +C_{31} 22S and C_{31} 22R)Hopanes

Hopanes 31Hops = C_{31} (S+R) Hopane/ (C_{29} + C_{30} +C_{31} 22S and C_{31} 22R)Hopanes